# Detection of Low-Concentration Biological Samples Based on a QBIC Terahertz Metamaterial Sensor

Bing Dong , Bo Wei , Dongshan Wei * , Zhilin Ke , Dongxiong Ling *

Posted Date: 15 May 2024

doi: 10.20944/preprints202405.1030.v1

Keywords: Terahertz; Metamaterial sensor; Quasi-bound state in the continuum; Lithium citrate; Bovine serum albumin; Limit of detection

*Article*

# Detection of Low-Concentration Biological Samples Based on a QBIC Terahertz Metamaterial Sensor

**Bing Dong [1,2], Bo Wei [3], Dongshan Wei [4,*], Zhilin Ke [1] and Dongxiong Ling [1,*]**

[1] School of Electrical Engineering and Intelligentization, Dongguan University of Technology, Dongguan, Guangdong, 523808, China
[2] College of Electronics and Information Engineering, Shenzhen University, Shenzhen, Guangdong, 518060, China
[3] School of Physics and Optoelectronic Engineering, Yangtze University, Jingzhou, Hubei. 434023, China
[4] Shenzhen Institute of Advanced Technology, Chinese Academy of Sciences, Shenzhen, Guangdong, 518055, China
* Correspondence: ds.wei@siat.ac.cn (D.W.); lingdx@dgut.edu.cn (D.L.)

**Abstract:** Quasi-bound state in the continuum (QBIC) can effectively enhance the interaction of terahertz (THz) wave with matters due to the tunable high-Q property, which has a strong potential application in detection of low-concentration biological samples in the THz band. In this paper, a novel THz metamaterial sensor with a double-chain separated resonant cavity structure based on QBIC is designed and fabricated. The process of excitation of the QBIC mode is verified and the structural parameters are optimized after considering the ohmic loss by simulations. The simulated refractive index sensitivity of the sensor is up to 544 GHz/RIU, much higher than those of recently reported THz metamaterial sensors. Sensing sensitivity of the proposed metamaterial sensor is confirmed in experiment by detecting low-concentration lithium citrate (LC) and bovine serum albumin (BSA) solutions. The limits of detection (LoDs) are obtained to be 0.0025 mg/mL (12 μM) for LC and 0.03125 mg/mL (0.47 μM) for BSA, respectively, both of which excel over most of reported results in previous studies. These results indicate that the proposed THz metamaterial sensor has excellent sensing performances and can well be applied to the detection of low concentration biological samples.

**Keywords:** terahertz; metamaterial sensor; quasi-bound state in the continuum; lithium citrate; bovine serum albumin; limit of detection

## 1. Introduction

Terahertz (THz) wave has great potential for substance detection by virtue of its broadband, low-energy, and unique fingerprint spectrum [1–4]. However, with the improvement of the required detection accuracy, the amount of reagents and the concentration of the test samples are often at the micro- or even trace level, resulting in the traditional THz detection technology having problems such as weak response to substances and difficulty in capturing the spectrum. To address these problems, many structures and devices including micro- and nanofluidics [5–7], attenuated total reflection(ATR) [8], and micro- and nanostructures [9] have been proposed and applied to enhance THz spectral signals to some extent. However, the enhancement to THz spectroscopy detections of very low-concentration biological samples is still limited.

As an artificial composite material, metamaterials have unique properties which are not found in natural materials [10–12]. Metamaterials can interact with incident THz wave and stimulate the directional movement of surface electrons, so that the metamaterials can realize the enhancement of THz wave within the local area, and thus capture more information about the light-matter interaction [13]. THz metamaterial enhancement performances can be characterized by the Q factor and the sensitivity *S*. High Q factor and high sensitivity have been the unremitting pursuit in the field of THz

 doi:10.20944/preprints202405.1030.v1



spectroscopy detection. Conventional metamaterial design methods such as surface plasmon resonance (SPR) [14], Fano resonance [15], electromagnetically induced transparency (EIT) [16,17] and Mie resonance [18,19], are difficult to achieve both high Q factor and high sensitivity.

Bound state in the continuum (BIC) is a wave that remains localized even though it coexists with a continuous spectrum of the radiation wave that can carry energy away [20], i.e., it is an eigenmode without electromagnetic energy leakage [21,22], and hence its theoretical Q factor can reach infinity. While quasi-bound state in the continuum(QBIC) makes a small portion of the electromagnetic energy leakage to the far field by introducing a structural asymmetry into the BIC mode [23]. By controlling the asymmetry it is possible to control the degree of electromagnetic energy leakage and thus actively regulate the Q factor [24–26], which provides an important idea of designing metamaterials sensors with adjustable high Q factors.

Since its potential feasibility of achieving both high-Q and high-sensitivity detection of low-concentration samples, the THz metamaterial sensor based on QBIC has been a research hotspot recently. Some of representative works in the latest two years are briefly introduced as follows. In 2023, Chang and Du et al. [27] presented a chip-based portable ultra-sensitive THz metasensor comprised of the split-ring resonator metasurface which supports magnetic dipole QBIC combining functionalized gold nanoparticles (AuNPs) and used this metasensor to detect ultralow concentration of C-reactive protein and Serum Amyloid A protein down to 1 pM. Wang et al. [28] proposed a distinctive 2.5D out-of-plane architectures based plasmonic symmetry protected (SP)-BIC metasurfaces and demonstrates a detection limit of endotoxin as low as 0.01 EU $mL^{-1}$. Liu et al. [29] manipulated the interference coupling between electric quadrupole and magnetic dipole in the metallic metasurface to excite ultrahigh quality QBIC with the Q factor of up to 503 and used this metasurface to detect trace homocysteine (Hcy) molecules to obtain a limit of detection of 12.5 pmol/μL, which is about 40-times better than that of the classical Dipole mode. In 2024, Zhong et al. [30] prepared a THz QBIC metamaterial sensor based on an all-silicon dielectric material with periodically etching grooves and holes on the surface and obtained a QBIC mode with a high Q factor. Using the sensor to detect amino acid molecules, they obtained a lowest detection quantitation of 8.7 nmol. Huang et al. [31] reported a novel terahertz (THz) biosensor based on the integration of QBIC with graphene to discern concentrations of ethanol and N-methylpyrrolidone in a wide range from 100% to 0% with the lowest detection concentration value of 0.21 pg/mL.

In this paper, a novel THz metamaterial sensor comprised of a dual-chain separated resonant cavity structure on a substrate based on QBIC is designed and fabricated and its sensing performances are analyzed and tested in simulation and experiment. The rest of this paper is organized as follows. In Section 2, the THz metamaterial sensor is designed and the related sensing performances are discussed by simulations. In Section 3, the sensor is fabricated and the THz spectroscopy measurement method is introduced. In Section 4, the THz metamaterial sensing experiments of two biological samples are performed and the results are discussed. In Section 5, conclusions of this work are given.

## 2. Design and Sensing Performance Simulations

### *2.1. Structural Design of the Metamaterial Sensor*

The designed metamaterial sensor is shown in Figure 1 and its unit structure comprised of metal double-chain separated resonant cavities is pointed out by the blue arrow in Figure 1 with structural sizes of $P_1$ = 40 μm , $P_2$ = 80 μm, $l_1$ = 3 μm, $l_2$ = 28 μm, $d$ = 30 μm and $d_1$ = 2 μm and the thickness of 200 nm. The substrate of the metamaterial sensor is high-purity quartz with a thickness of $W$ = 500 μm. Symmetry-protected excitation of QBIC is broken by varying the magnitude of $d_2$.

Preprints.org (www.preprints.org) | NOT PEER-REVIEWED | Posted: 15 May 2024 doi:10.20944/preprints202405.1030.v1



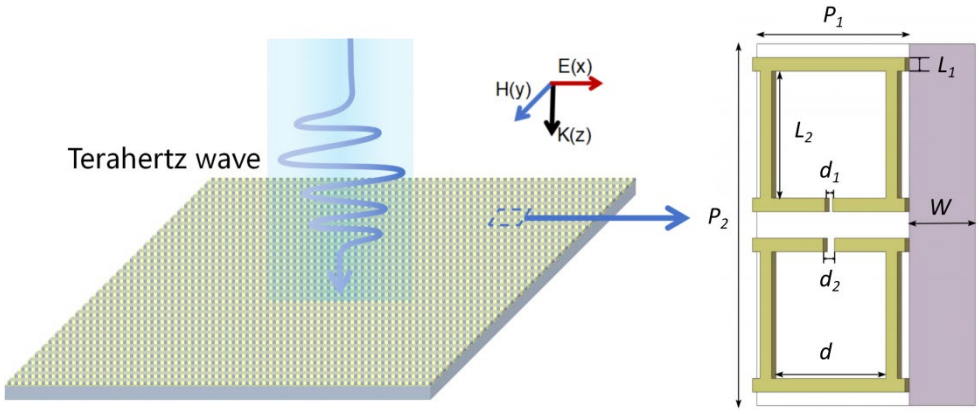


**Figure 1.** Structure of the sensor.

All of the simulations in this work are performed with the CST studio software. As shown in Figure 2a, under the excitation of vertically incident THz wave, the upper and lower resonance cavities generate a pair of reverse currents (blue arrows), which produce a circular magnetic field (violet arrows). The electric field distribution at the openings is demonstrated in the dashed box of Figure 2a. The magnetic field generated by the upper and lower loops is coupled in the resonance cavities and their gap region, thus exhibiting a binding force on the photons and resulting in confinement of the light field in a large area around the loops and the resonance cavities as shown in Figure 2b, which may ensure the sensor can capture more sample molecules on the surface and realize the trace detection of samples.

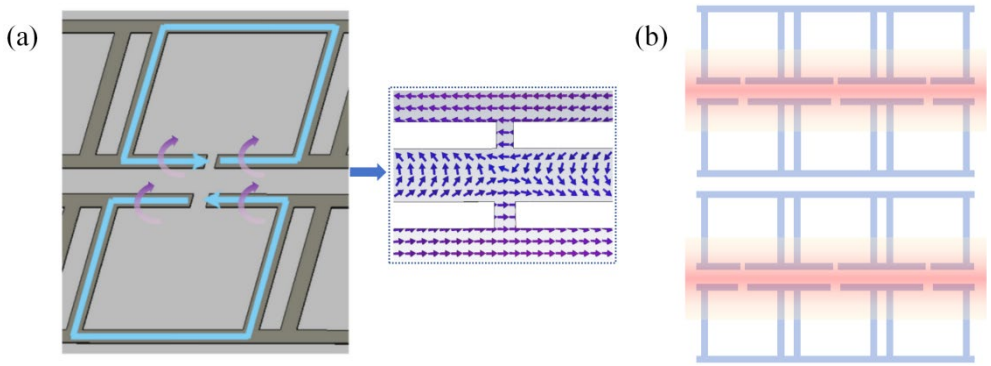


**Figure 2.** (**a**) Current and electromagnetic fields on the surface of the sensor; (**b**) Schematic of the constrained light field.

*2.2. QBIC Characteristics and Performance Optimization*

In order to verify the formation mechanism of QBIC modes, the metamaterial surface structure was simulated using a PEC material to eliminate the effects of the ohmic loss[32]. Keeping the width $d_1$ constant and increasing the width $d_2$ from 0.5 to 4.0 μm, the degree of asymmetry $\alpha = (d_2-d_1)/2$ is defined and varies from -0.75 to 1.

When the THz wave radiates on the surface of the metamaterial sensor in the TM mode, variation of the transmission resonant peak with the degree of asymmetry is shown in Figure 3a. When $\alpha = 0$, the resonant peak cannot be observed in the spectrum. At this time, the sensor structure is in the symmetry-protected BIC mode and the energy is bound in the near-field and not leaking into the free space. Therefore, the Q factor is infinite, which causes the resonant peak in the spectrum with an infinitely narrow linewidth cannot be observed. When $\alpha \neq 0$, a resonance peak with a narrow line width is observed near the BIC mode, and the line width gradually increases with the increase of $|\alpha|$ due to the fact that the introduction of $\alpha$ breaks the symmetry of the original structure, leading to the transformation of the BIC mode with no energy leakage into the QBIC mode with partial energy

 doi:10.20944/preprints202405.1030.v1



leakage. The magnetic field energy at one of the openings is monitored in both BIC and QBIC modes as shown in Figure 3b. No magnetic field energy is observed in the BIC mode, while magnetic field energy leakage is observed around the structure in the QBIC mode, which verifies the transformation from BIC into QBIC.

Meanwhile, the relationship between the Q factor and the degree of asymmetry $\alpha$ is explored and the result is fitted with the Fano formula[33]:

$$T_{Fano} = t_0 \times |a_1 + ia_2 + \frac{b}{\omega - \omega_0 + i\gamma}|^2$$

where $a_1$, $a_2$ are real numbers, $\omega_0$ and $\gamma$ are the resonant frequency and damping rate, respectively, and the Q factor of the Fano resonance is calculated under different $\alpha$ according to $Q = \omega_0/2\gamma$. Variation of the Q factor with $|\alpha|$ is obtained as shown in Figure 3c. It can be seen that the closer $|\alpha|$ is to 0, the larger the Q factor is. Furthermore, the Q factors are approximately the same at the same $|\alpha|$. Previous studies had confirmed that the relation between the Q factor and $\alpha$ is inversely quadratic [34,35] with $Q = Q_1|\alpha|^{-2}$, where $Q_1$ is an independent constant and depends on the topology and material properties of the metamaterial itself. Here, the Q factor is fitted with the equation of $Q = 98.96|\alpha|^{-2}$ with $R^2 > 0.999$. This is in accordance with the Q factor variation rule for the excitation of the symmetry-protected BIC mode, proving that the QBIC mode is excited by symmetry-breaking.

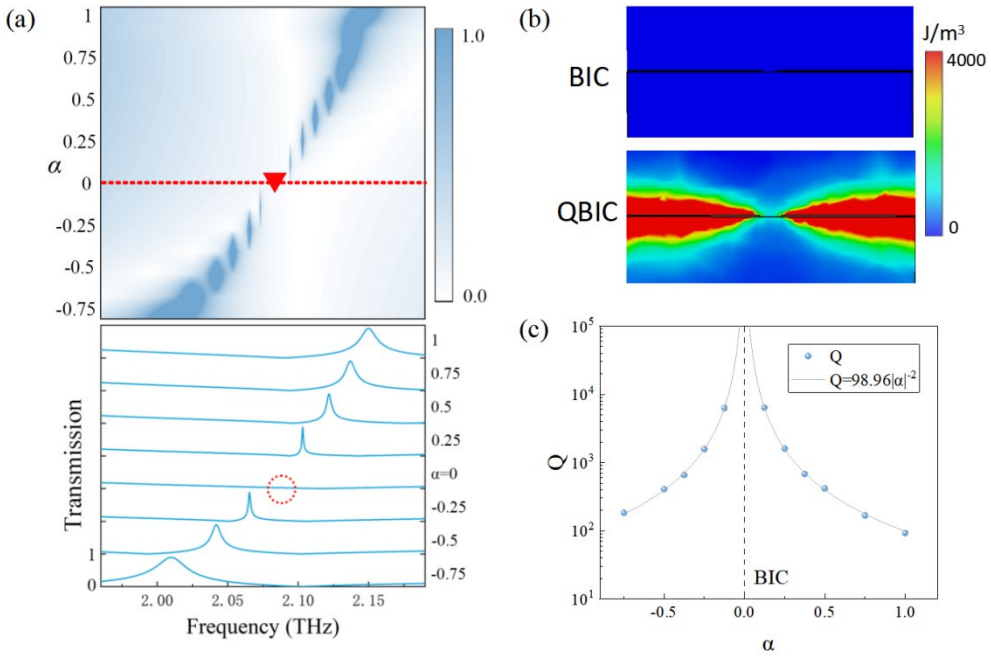


**Figure 3.** (**a**) The evolution of the resonance peak; (**b**) Magnetic field energy at one of the openings; (**c**) Q varies with $\alpha$.

In the above simulations, the ideal conducting material of PEC was chosen to verify the relationship between Q and $\alpha$, while the effect of the ohmic loss on the resonant strength is neglected[32]. To investigate the ohmic loss of the metal structure sensor, keeping $d_1 = 2$ μm constant, increasing $d_2$ from 3 to 9 μm, i.e., $\alpha$ increasing from 0.5 to 3.5, variations of the resonant peak intensity with $\alpha$ for the PEC sensor and for the gold (conductivity: 4.1×107 S/m) sensor are shown in Figs. 4a and b, respectively for comparison. From these two figures, we can see there is obvious difference in the resonant peak between the PEC and metal sensors. To quantitatively show the ohmic loss on the sensor, the Q factors at different $\alpha$ are plotted for comparison as shown in Figure 4c. It can be seen that the Q factor decreases as $\alpha$ increases. To determine the optimal structural asymmetry, a figure of merit (FoM) of the simulated sensor is defined as $FoM = Q \times H$, where $H$ is the depth of the resonant peak as shown in the inset of Figure 4d. The relation between the calculated FoM and $\alpha$ is shown in Figure 4d. It can be seen that at $\alpha = 2$, FoM reaches the maximal value, so $\alpha = 2$ is adopted as the

 doi:10.20944/preprints202405.1030.v1



structural asymmetry with $d_1$ = 2 μm and $d_2$ = 6 μm in the following simulations. At this time, the Q factor has about a 30% decrease due to the ohmic loss seen from Figure 4c.

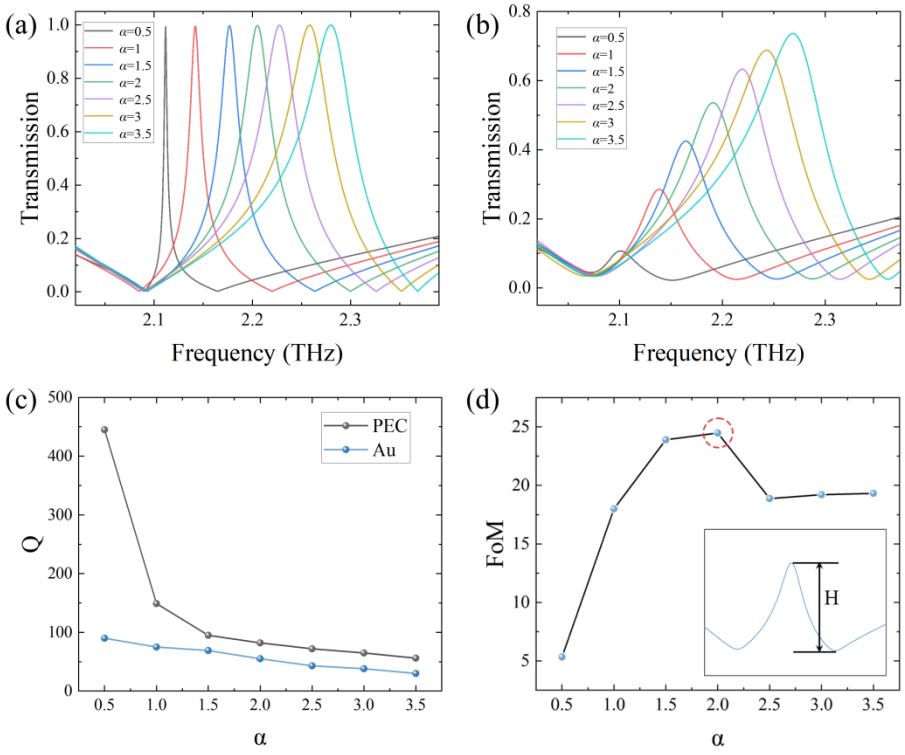


**Figure 4.** (**a**)Resonant peak variation with $\alpha$ using the PEC material; (**b**)Resonance peak variation with $\alpha$ using the gold metal material; (**c**)Variation of Q factor with $\alpha$ for different materials; (d)Variation of FoM with $\alpha$ and the definition of H in the inset.

*2.3. Sensing Performance Simulations*

To characterize the sensing performances of the metamaterial sensor, transmission spectra under different thicknesses and refractive indices of the detected sample are simulated and shown in Figs. 5a and c. It can be seen that in comparison with the resonant frequency of the blank sensor, the resonant frequencies of the sensor covered by the sample with different thicknesses and refractive indices have different redshifts. The reason is due to that the increased thickness and refractive index of the detected sample will increase the equivalent capacitance of the sensor, which will result in the decrease of the resonant frequency according to the LC circuit principle. To quantitatively illustrate the effects of the thickness and the refractive index of the detected sample on the transmission property of the sensor, the relations between the resonant frequency shift $\Delta f$ and the thickness $h$ are shown in Figure 5b. From this figure, we can see that $\Delta f$ first nonlinearly increases with the increase of $h$ and then saturates at 20 μm. This is due to the fact that as the thickness of the covered sample increases to exceed 20 μm, the upper part of the sample exceeding the edge of the bound optical field cannot interact with the confined electromagnetic wave, and therefore the thickness sensitivity disappears. From Figure 5d, we can see the resonant frequency shift $\Delta f$ increases linearly with the increase of $\Delta n$ at different sample thicknesses, where $\Delta n$ is the refractive index change relative to the air of $n$ = 1.0. By defining the sensitivity of the sensor as $S = \Delta f/\Delta n$, it can be seen that the maximal $S$ is calculated to be 544 GHz/RIU at the saturated covering thickness of 20 μm. Even at the smallest simulation thickness of $h$ = 1 μm, $S_1$ = 220 GHz/RIU as shown in Figure 5d, indicating that the sensor also has good sensing performance for ultra-thin object detection.

Preprints.org (www.preprints.org) | NOT PEER-REVIEWED | Posted: 15 May 2024 doi:10.20944/preprints202405.1030.v1



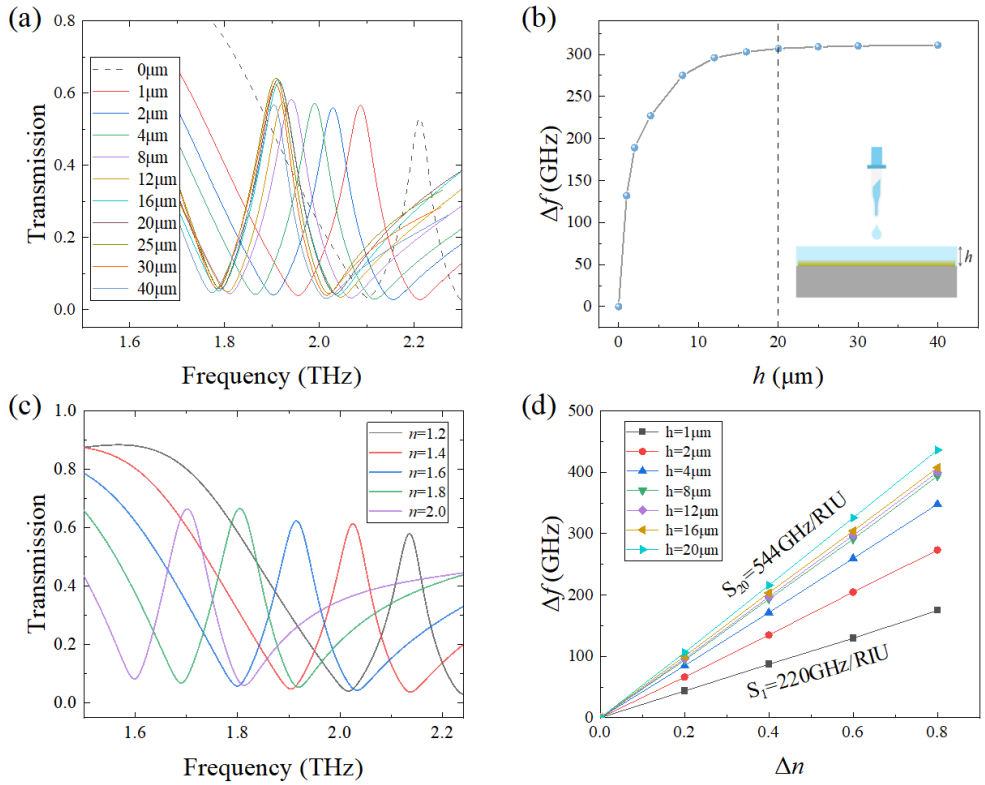


**Figure 5.** (**a**)Frequency shift varies with thickness of the detected sample; (**b**)relations between the resonant frequency shift and the thickness; (**c**)Frequency shift with refractive index at $h$ = 20 μm; (**d**)Refractive index sensitivity at different thicknesses.

To evaluate the sensing performance of the designed metamaterial sensor, the S parameters for different sensors reported in recent literature are listed in Table 1 for comparison. It can be seen that the sensitivity of the designed sensor is excellent.

**Table 1.** Simulated refractive index sensitivity of the metamaterial sensor.

| Structures | S (GHz/RIU) | Reference |
|---|---|---|
| Metal rings and double "I" cross structure | 300 | [36] |
| Asymmetric open ring | 328 | [37] |
| Gold nanoparticles and gold wires | 123.45 | [38] |
| QBIC-Fano Resonance | 165 | [39] |
| Double elliptic QBIC structure | 293 | [40] |
| Periodic array of two ring chain resonators | 420 | [29] |
| Double-chain resonant cavity QBIC | 544 | This work |

## 3. Experimental Methods

### *3.1. THz Spectroscopy Equipment*

All THz spectroscopy measurements in this work were performed using a THz time-domain spectroscopy (THz–TDS) spectrometer (Advantest Photonix TAS7500SU, Advantest Corporation,

 doi:10.20944/preprints202405.1030.v1



Tokyo, Japan). During THz spectroscopy measurements, a maximal delay time of 132 ps was set and a frequency resolution of 7.6 GHz was obtained. Under the setting, this spectrometer can stably produce a spectrum every 200 ms. The THz-TDS spectrometer is equipped with a dry air purge accessory with which the humidity of the detection chamber can be controlled around 5%. All THz spectroscopy measurements were performed in the transmission mode at a temperature of 23.0 ± 1.0°C.

### *3.2. Fabrication of Metamaterial Sensor*

According to the above simulation results, the metamaterial sensor with optimal parameters was fabricated using a combination of photolithography and vapor deposition processes. In order to bond the metal layer and the substrate more tightly, 10-nm-thick chromium is added between the 200-nm gold metal layer and the 500-μm quartz substrate as an adhesive. One of the fabricated metamaterial sensors is shown in Figure 6a. THz Transmission spectrum of the fabricated sensor is displayed in Figure 6b. For comparsion, the simulation transmission spectrum of the blank sensor is also shown. It can be seen that the resonant peak of the fabricated sensor has a blueshift of about 80 GHz and its depth is smaller compared to the simulated resonant peak, which may be due to the facts that the actual ohmic loss of the metal is higher than the simulated one and the quality of the experimental resonant peak degrades because of the impact of the processing accuracy.

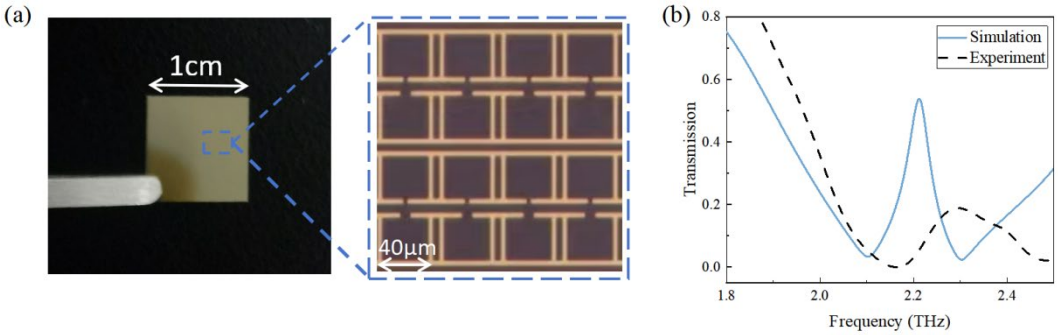


**Figure 6.** (**a**) Photograph of the metamaterial sensor;(**b**) Simulation and experimental spectra of the blank metamaterial sensor.

### *3.3. Biological Sample Preparation*

Two typical biological samples were prepared and tested in this work. One is Lithium citrate (chemical formula: $Li_3C_6H_5O_7$, molecular weight: 209.92), which is widely used in the clinical treatment of psychosis and bi-directional affective disorder[41]. The other is Bovine serum albumin (BSA), which is a white to light yellow lyophilized powder with a molecular weight of 66.44 kDa and a solubility of 100 mg/mL. Both of these two samples with purity > 99.0% were purchased from Macklin corporation(Shanghai, China) without further purification.

To prepare Lithium citrate (LC) solutions with different concentrations, 0.2 g LC sample is weighed and dissolved in 100 mL deionized water to obtain the concentration of 2 mg/mL. To obtain lower concentration samples, the 2 mg/mL solution was sequentially diluted to 1.0, 0.1, 0.01 and 0.0025 mg/mL. Similarly, to obtain the BSA solution samples, 0.1 g of BSA sample is weighed and dissolved in 100 mL of deionized water to obtain the concentration of 1.0 mg/mL, then the 1.0 mg/mL BSA solution was diluted to obtain 0.5, 0.25, 0.125, 0.0625, and 0.03125 mg/mL solutions.

To perform the THz spectroscopy measurement, one of the 20-μL liquid samples with different concentrations was firstly dropped using a pipette on the surface of the metamaterial sensor and was evenly spread using a homogenizer. Then drying of the liquid sample on the surface of the metamaterial sensor was executed in an oven at a temperature of 40℃ for about 5 hours. Each sample was measured for three times to minimize the experimental error.

 doi:10.20944/preprints202405.1030.v1



## 4. Experimental Results and Discussion

### *4.1. Detection of Lithium Citrate Based on the Metamaterial Sensor*

Transmission spectra of LC solutions at different concentrations are shown in Figure 7a. It can be observed that the central frequency of the resonant peak has a redshift as the concentration of the LC sample increases. To quantitatively describe the resonant frequency redshift, variation of $\Delta f$ with the concentration is shown in Figure 7b and the relation between them can be well linearly fitted with an equation of y = 118.88 x + 31.40 with $R^2$ = 0.97. Due to the spectral resolution of the spectrometer (7.6 GHz), when the LC concentration is 0.0025 mg/mL, $\Delta f$ reduces to the equivalent value with the spectral resolution as shown in Figure 7b. Therefore, the limit of detection (LoD) of LC by the metamaterial sensor is determined to be 0.0025 mg/mL (~ 12 μM). In comparison to the recent detection result of 0.1 mM[42] for potassium citrate with the traditional THz metamaterial, the QBIC THz metamaterial has one order of magnitude improvement on the LoD. In addition, the liquid amount dropped on the sensor is only 20 μL, which is also significantly reduced compared with previous THz metamaterial detection[37], indicating the QBIC metamaterial sensor in this work has excellent sensing performance.

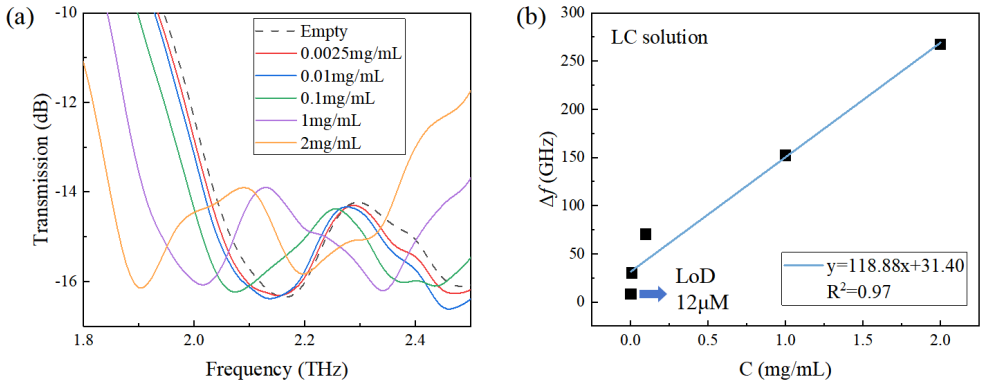


**Figure 7.** (**a**) THz transmission spectra of LC solutions at different concentrations; (**b**)Variation of $\Delta f$ with the concentration.

### *4.2. Detection of BSA Based on the Metamaterial Sensor*

THz transmission spectra of BSA solutions with different concentrations were measured and the results were shown in Figure 8a. Similarly, the central frequency of the resonant peak has a redshift as the concentration of the BSA sample increases. The relation between the central resonant frequency shift and the BSA concentration can be linearly fitted with an equation of y = 104.85 x + 12.59 with $R^2$ = 0.98 as shown in Figure 8b. Similarly, considering the spectral resolution of the spectrometer, the LoD of the metamaterial sensor for BSA solutions is 0.03125 mg/mL (0.47 μM) as marked in Figure 8b. To compare of this LoD with previously reported detection results of 1.52 μM by a polarization-insensitive THz sensor [43], 1 μM by a asymmetric split resonator THz sensor [42], 0.53 μM by a all-metal THz sensor [44] and 0.15 μM by a SRRs THz sensor [45], the QBIC sensor is advantageous in sensitivity for low-concentration protein detection.

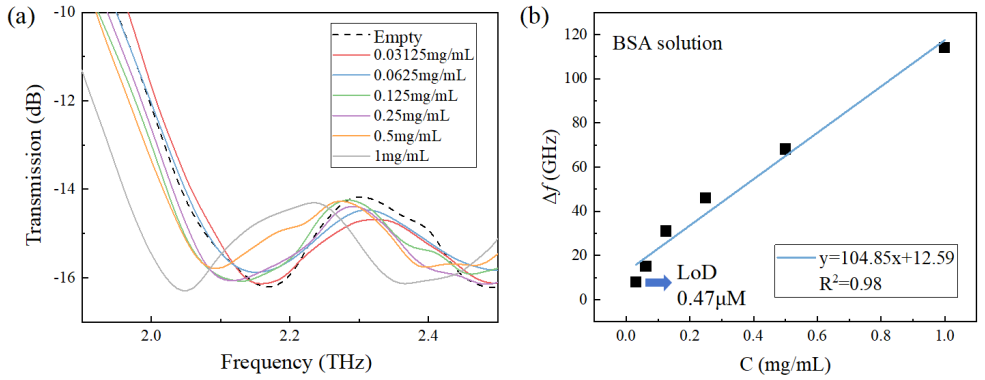

 doi:10.20944/preprints202405.1030.v1



**Figure 8.** (a)THz transmission spectra of BSA solutions at different concentrations; (b)Variation of $\Delta f$ with the concentration.

## 4. Conclusions

In summary, we designed and fabricated a THz metamaterial sensor based on the bound state in the continuum with a double chain-type separated resonance cavity structure. By controlling the size of the openings, an asymmetry is introduced into the structure. Distribution of electric and magnetic fields on the surface of the metamaterial sensor was simulated and the introduction of the asymmetry degree exciting the mode transformation from BIC to QBIC was verified. The thickness and refractive index sensitivities of the sensor were investigated and the saturated sample thickness and the highest refractive index sensitivity of the sensor were determined to be around 20 μm and 544 GHz/RIU, respectively by simulations. In addition, the effect of ohmic loss on the metamaterial sensor was also discussed. Since the ohmic loss of the gold metal, the Q factor of the sensor decreases 30% compared with the PEC material. In experiment, the detection capability of the metamaterial sensor for low-concentration biological samples was verified. For lithium citrate solution detection, the LoD was determined to be 0.0025 mg/mL (12μM), which is one order of magnitude lower than the previous report. For BSA solution detection, the LoD was 0.03125 mg/mL (0.47 μM), greatly lower than the reported results using traditional THz sensors. Meanwhile, the amount of liquid required for a single detection is only 20 μL, also much lower than the requirements in the previous studies. Therefore, the proposed THz metamaterial sensor based on the QBIC mode has excellent sensing sensitivities and can be used for detection of low-concentration biological samples.

**Author Contributions:** Conceptualization, W.D.S. and L.D.X.; methodology, D.B. and W.B.; software, K.Z.L.; validation, W.D.S.; formal analysis, D.B. and W.D.S.; investigation, D.B., W.B. and K.Z.L.; sources, W.D.S. and L.D.X.; data curation, D.B.; writing—original draft preparation, D.B.; writing—review and editing, W.D.S.; visualization, D.B.; supervision, W.D.S. and L.D.X.; project administration, W.D.S. and L.D.X.; funding acquisition, W.D.S. and L.D.X. All authors have read and agreed to the published version of the manuscript.

**Funding:** This work has been partially supported by the Major Instrumentation Development Program of the Chinese Academy of Sciences (ZDKYYQ20220008) and Guangdong Basic and Applied Basic Research Foundation (2021B1515140018).

**Data Availability Statement:** Data underlying the results presented in this paper are not publicly available at this time but may be obtained from the authors upon reasonable request.

**Conflicts of Interest:** There are no conflicts of interest to declare.

## References

1. Y. Peng, C. Shi, Y. Zhu, M. Gu, S. Zhuang, Terahertz spectroscopy in biomedical field: a review on signal-to-noise ratio improvement, PhotoniX, 1 (2020) 1-18.
2. A. D'Arco, M. Di Fabrizio, V. Dolci, M. Petrarca, S. Lupi, THz pulsed imaging in biomedical applications, Condensed Matter, 5 (2020) 25.
3. H. Yan, W. Fan, X. Chen, L. Liu, H. Wang, X. Jiang, Terahertz signatures and quantitative analysis of glucose anhydrate and monohydrate mixture, Spectrochimica Acta Part A: Molecular and Biomolecular Spectroscopy, 258 (2021) 119825.
4. S. Jun, Y. Ahn, Terahertz thermal curve analysis for label-free identification of pathogens, Nature Communications, 13 (2022) 3470.
5. K. Shih, P. Pitchappa, L. Jin, C.H. Chen, R. Singh, C. Lee, Nanofluidic terahertz metasensor for sensing in aqueous environment, Applied Physics Letters, 113 (2018) 071105.
6. L. Liang, X. Hu, L. Wen, Y. Zhu, X. Yang, J. Zhou, Y. Zhang, I.E. Carranza, J. Grant, C. Jiang, Unity integration of grating slot waveguide and microfluid for terahertz sensing, Laser & Photonics Reviews, 12 (2018) 1800078.
7. Z. Geng, X. Zhang, Z. Fan, X. Lv, H. Chen, A route to terahertz metamaterial biosensor integrated with microfluidics for liver cancer biomarker testing in early stage, Scientific reports, 7 (2017) 16378.
8. K. Shiraga, Y. Ogawa, N. Kondo, A. Irisawa, M. Imamura, Evaluation of the hydration state of saccharides using terahertz time-domain attenuated total reflection spectroscopy, Food Chemistry, 140 (2013) 315-320.

 doi:10.20944/preprints202405.1030.v1




9. M. Theuer, R. Beigang, D. Grischkowsky, Highly sensitive terahertz measurement of layer thickness using a two-cylinder waveguide sensor, Applied Physics Letters, 97 (2010) 071106.
10. G. Dolling, C. Enkrich, M. Wegener, C.M. Soukoulis, S. Linden, Simultaneous negative phase and group velocity of light in a metamaterial, Science, 312 (2006) 892-894.
11. H. Yao, X. Yan, M. Yang, Q. Yang, Y. Liu, A. Li, M. Wang, D. Wei, Z. Tian, L. Liang, Frequency-dependent ultrasensitive terahertz dynamic modulation at the Dirac point on graphene-based metal and all-dielectric metamaterials, Carbon, 184 (2021) 400-408.
12. Z. Li, W. Liu, G. Geng, Z. Li, J. Li, H. Cheng, S. Chen, J. Tian, Multiplexed nondiffracting nonlinear metasurfaces, Advanced Functional Materials, 30 (2020) 1910744.
13. Z. Zhang, M. Yang, X. Yan, X. Guo, J. Li, Y. Yang, D. Wei, L. Liu, J. Xie, Y. Liu, L. Liang, J. Yao, The Antibody-Free Recognition of Cancer Cells Using Plasmonic Biosensor Platforms with the Anisotropic Resonant Metasurfaces, Acs Applied Materials & Interfaces, 12 (2020) 11388-11396.
14. M.S. Islam, J. Sultana, M. Biabanifard, Z. Vafapour, M.J. Nine, A. Dinovitser, C.M.B. Cordeiro, B.W.H. Ng, D. Abbott, Tunable localized surface plasmon graphene metasurface for multiband superabsorption and terahertz sensing, Carbon, 158 (2020) 559-567.
15. C. Blanchard, J.P. Hugonin, C. Sauvan, Fano resonances in photonic crystal slabs near optical bound states in the continuum, Phys.rev.b, 94 (2016) 155303.
16. Active control of electromagnetically induced transparency analogue in terahertz metamaterials, Nature Communications, 3 (2012) 1151.
17. J. Wu, B. Jin, J. Wan, L. Liang, Y. Zhang, T. Jia, C. Cao, L. Kang, W. Xu, J. Chen, Superconducting terahertz metamaterials mimicking electromagnetically induced transparency, Applied Physics Letters, 99 (2011) 36.
18. Y. Wu, L. Kang, H. Bao, D.H. Werner, Exploiting Topological Properties of Mie-Resonance-Based Hybrid Metasurfaces for Ultrafast Switching of Light Polarization, ACS Photonics, 7 (2020) 2362-2373.
19. S. Park, J. Cho, D. Jeong, J. Jo, M. Nam, H. Rhee, J.S. Han, Y.J. Cho, B.-K. Ju, D.-H. Ko, Simultaneous enhancement of luminescence and stability of CsPbBr3 perovskite nanocrystals via formation of perhydropolysilazane-derived nanopatterned film, Chemical Engineering Journal, 393 (2020) 124767.
20. C.W. Hsu, B. Zhen, A.D. Stone, J.D. Joannopoulos, M. Soljačić, Bound states in the continuum, Nature Reviews Materials, 1 (2016) 1-13.
21. J. Wang, P. Li, X. Zhao, Z. Qian, X. Wang, F. Wang, X. Zhou, D. Han, C. Peng, L. Shi, Optical bound states in the continuum in periodic structures: mechanisms, effects, and applications, Photonics Insights, 3 (2024) R01.
22. H. Zhong, T. He, Y. Meng, Q. Xiao, Photonic Bound States in the Continuum in Nanostructures, Materials, 16 (2023) 7112.
23. A.S. Kupriianov, Y. Xu, A. Sayanskiy, V. Dmitriev, Y.S. Kivshar, V.R. Tuz, Metasurface engineering through bound states in the continuum, Physical Review Applied, 12 (2019) 014024.
24. S. Romano, G. Zito, S.N.L. Yepez, S. Cabrini, E. Penzo, G. Coppola, I. Rendina, V. Mocella, Tuning the exponential sensitivity of a bound-state-in-continuum optical sensor, Optics Express, 27 (2019) 18776-18786.
25. S. Romano, M. Mangini, E. Penzo, S. Cabrini, A.C. De Luca, I. Rendina, V. Mocella, G. Zito, Ultrasensitive Surface Refractive Index Imaging Based on Quasi-Bound States in the Continuum, Acs Nano, 14 (2020) 15417-15427.
26. J.W. Yoon, S.H. Song, R. Magnusson, Critical field enhancement of asymptotic optical bound states in the continuum, Scientific reports, 5 (2015) 18301.
27. R. Wang, L. Xu, L. Huang, X. Zhang, H. Ruan, X. Yang, J. Lou, C. Chang, X. Du, Ultrasensitive Terahertz Biodetection Enabled by Quasi-BIC-Based Metasensors, Small, 19 (2023) 2301165.
28. Z. Wang, J. Sun, J. Li, L. Wang, Z. Li, X. Zheng, L. Wen, Customizing 2.5 D Out-of-Plane Architectures for Robust Plasmonic Bound-States-in-the-Continuum Metasurfaces, Advanced Science, 10 (2023) 2206236.
29. B. Liu, Y. Peng, Z. Jin, X. Wu, H. Gu, D. Wei, Y. Zhu, S. Zhuang, Terahertz ultrasensitive biosensor based on wide-area and intense light-matter interaction supported by QBIC, Chemical Engineering Journal, 462 (2023) 142347.
30. T. Lin, Y. Huang, S. Zhong, T. Shi, F. Sun, Y. Zhong, Q. Zeng, Q. Zhang, D. Cui, Passive trapping of biomolecules in hotspots with all-dielectric terahertz metamaterials, Biosensors & bioelectronics, 251 (2024) 116126.

 doi:10.20944/preprints202405.1030.v1




31. C. Huang, L. Liang, P. Chang, H. Yao, X. Yan, Y. Zhang, Y. Xie, Terahertz Liquid Biosensor Based on A Graphene Metasurface for Ultrasensitive Detection with A Quasi-Bound State in the Continuum, Advanced Materials, 36 (2024) 2310493.
32. D.Ö. Güney, T. Koschny, C.M. Soukoulis, Reducing ohmic losses in metamaterials by geometric tailoring, Physical Review B, 80 (2009) 125129.
33. S. Yang, C. Hong, Y. Jiang, J.C. Ndukaife, Nanoparticle Trapping in a Quasi-BIC System, ACS Photonics, 8 (2021) 1961-1971.
34. K. Kirill, L. Sergey, L. Mingkai, B. Andrey, K. Yuri, Asymmetric Metasurfaces with High-Q Resonances Governed by Bound States in the Continuum, Physical review letters, 121 (2018) 193903.
35. L. Cong, R. Singh, Symmetry-protected dual bound states in the continuum in metamaterials, Advanced Optical Materials, 7 (2019) 1900383.
36. J. Yang, M. Wang, H. De, Y. Kang, Z. Li, Q. Liu, L. Xiong, Z. Wu, W. Qu, L. Shang, Dual-band terahertz sensor based on metamaterial absorber integrated microfluidic, Acta Optica Sinica, 41 (2021) 2328001.
37. X. Deng, Y. Shen, B. Liu, Z. Song, X. He, Q. Zhang, D. Ling, D. Liu, D. Wei, Terahertz metamaterial sensor for sensitive detection of citrate salt solutions, Biosensors, 12 (2022) 408.
38. K. Yang, J. Li, M.L. de la Chapelle, G. Huang, Y. Wang, J. Zhang, D. Xu, J. Yao, X. Yang, W. Fu, A terahertz metamaterial biosensor for sensitive detection of microRNAs based on gold-nanoparticles and strand displacement amplification, Biosensors and Bioelectronics, 175 (2021) 112874.
39. R. Wang, L. Xu, J. Wang, L. Sun, Y. Jiao, Y. Meng, S. Chen, C. Chang, C. Fan, Electric Fano resonance-based terahertz metasensors, Nanoscale, 13 (2021) 18467-18472.
40. Q. Zeng, F. Hu, Y. Zhou, High Q-value terahertz metamaterial sensor based on double ellipse structure, Acta Optica Sinica, 41 (2021) 199-205.
41. E. Roberts, A case of chronic mania treated with lithium citrate and terminating fatally, The Medical journal of Australia, 2 (1950) 261-262.
42. Y. Shen, X. Li, J. Wang, H. Liu, J. Jing, X. Deng, D. Wei, Low-concentration biological sample detection using an asymmetric split resonator terahertz metamaterial, Photonics, MDPI, 2023, pp. 111.
43. X. Hou, X. Chen, T. Li, Y. Li, Z. Tian, M. Wang, Highly sensitive terahertz metamaterial biosensor for bovine serum albumin (BSA) detection, Optical Materials Express, 11 (2021) 2268-2277.
44. W. Gangqi, Z. Fengjie, L. Tingting, L. Jianjun, H. Zhi, Q. Jianyuan, All-metal terahertz metamaterial biosensor for protein detection, Nanoscale research letters, 16 (2021) 109-109.
45. H.M. Silalahi, Y.-P. Chen, Y.-H. Shih, Y.-S. Chen, X.-Y. Lin, J.-H. Liu, C.-Y. Huang, Floating terahertz metamaterials with extremely large refractive index sensitivities, Photonics Research, 9 (2021) 1970-1978.